Topological validation of morphology modeling by extended reverse Monte Carlo analysis

Katsumi Hagita[1] and Takashi Teramoto[2]
[1]*Department of Applied Physics, National Defense Academy, Yokosuka 239-8686, Japan*
[2]*Chitose Institute of Science and Technology, Chitose 066-8655, Japan*
(Received 30 June 2007; revised manuscript received 3 March 2008; published 15 May 2008)

A combination of reverse Monte Carlo (RMC) and computational homology is examined as a useful approach in connecting scattering experiments to mathematics for 3D morphology modeling. We develop a different method of morphology modeling from multiple two-dimensional (2D) scattering patterns of structure functions by RMC technique using coarse-grained particles. We perform RMC analysis for multiple 2D scattering patterns of the configuration generated from the surface equation of double gyroid morphology. Homology analysis enables us to classify complex three-dimensional morphologies by incorporating topologically invariant quantities, the so-called Betti numbers. It is demonstrated that RMC analysis reconstructs the DG morphology from multiple 2D scattering patterns.

DOI: 10.1103/PhysRevE.77.056704 PACS number(s): 02.70.Uu, 81.70.Tx, 61.43.Bn, 61.05.cf

I. INTRODUCTION

Characterization and visualization of nanostructured morphology in materials science have recently attracted much interest. The bulk structure is very important in understanding the origin of the functions of some nanosized materials. Modeling from real materials has valuable a contribution in its simulational and numerical studies. A subject matter in the surfactant and water systems, the kinetic pathway during the morphological transition via double gyroid (DG) morphology, has recently generated much interest [1]. Three-dimensional transmission electron microscopy (3D-TEM) is a powerful tool for direct observation of the nanostructure of thin samples whose depth is limited to a few ten nanometers [2]. In order to examine not surface but bulk structures of soft materials such as polymer composites and colloids, a method observing large scale structures of the order of a few ten nanometers to a few μm is needed. Small angle x-ray scattering (SAXS) experiments have been widely used to study large-scale structures in the bulk of soft materials [3]. One of the advantages of this approach is that recent time-resolved SAXS experiments can observe fast structural changes in short intervals (on the order of 100 ms). Two-dimensional (2D) patterns of structure functions $S(\boldsymbol{q}^{\perp})$ are usually observed by using imaging plates and charge-coupled device (CCD) detectors. $S(\boldsymbol{q}^{\perp})$ indicates the projections of the structure factors onto the plane $q^{\parallel}=0$ in Ewald sphere. Here, the $\boldsymbol{q}^{\perp}$ plane is perpendicular to the axis of the incident x rays.

There is a demand for a method of modeling large-scale structures consistent with the 2D structure functions $S(\boldsymbol{q}^{\perp})$, without incorporating prepared structures and/or the expert judgment. One possible candidate is the reverse Monte Carlo (RMC) analysis method which is used to model the amorphous structure of atoms under periodic boundary condition (PBC) [4–6]. Note that the structural model obtained from RMC analysis is consistent with a given structure factor. It is confirmed that it can be applied to large bulk structure modeling [7]. RMC analysis of the structure of colloidal aggregates is also performed by assuming that a particle corresponds to a colloid instead of an atom [8,9]. To treat general small angle scattering data, the most useful method was originally proposed by Svergun concerning the modeling of isolated macromolecules, such as proteins, in dilute solution. In this approach, a randomly shaped large particle is represented by an aggregate of smaller dummy atoms [10]. Recently, one of the authors has developed the extended RMC method for the 2D patterns, $S(\boldsymbol{q}^{\perp})$, of a uniaxial system [11]. This method has been used to estimate from their 2D patterns $S(\boldsymbol{q}^{\perp})$ of stretched rubbers the three-dimensional (3D) morphology of silica nanoparticles with a diameter of about 300 nm [12]. These 2D patterns are observed in time resolved 2D-USAXS (ultrasmall angle x-ray scattering) experiments using SPring-8 by Shinohara *et al.* [3].

The RMC method is also used in modeling a structure with local disorders in the periodic system. The average structure consists of many crystalline unit cells and instantaneous positions create disorders around this average structure. The RMC method is more suitable than Rietveld analysis and pattern fitting based on maximum entropy method [13,14] in estimating the structures of materials not highly ordered. In order to model weak disorder in atomic crystalline systems from powder diffraction data, *RMCpow* and *RMCprofile* are proposed [15,16]. In these methods, the modeled atoms in the PBC box possess both consistent Bragg peaks and the diffuse scattering intensities associated with either the long- or short-range order of the structures. For fitting of multiple unit cells, the weighting factors for Bragg peaks and the diffuse scattering intensities are important in order to save computing times.

The purpose of this paper is to demonstrate the extended RMC analysis for the multiple 2D scattering patterns of complex 3D morphologies. As the first step of RMC modeling, the computer-generated 2D patterns of the structure factors of one unit cell of the DG morphology are examined. The DG morphology plays a key role during the morphological transition in surfactant and water systems. Recently, Imai *et al.* have observed changes of 2D patterns of scattering intensity in the various directions during the morphological transition via the DG morphology [1]. We have also developed techniques to apply computational homology for the topological characterization of the bulk structures consisting of an aggregate of particles. The identification of the DG mor-

phology, which belongs to the $Ia\bar{3}d$ space group, was difficult in the microphase separation system of diblock copolymers [17–21]. Instead of visual inspection of 3D pictures or cross-sectional views, the concept of algebraic topology provides us definitive identification in terms of the homology groups $H_k(U)$ $(k=0,\ldots,3)$ to characterize the topological properties of a 3D structure U [22]. In particular, the kth Betti number $\beta_k(U)$ is a rank of the kth homology group $H_k(U)$ of a topological space. $\beta_0(U)$ represents the number of connected components; $\beta_1(U)$ and $\beta_2(U)$ are equal to the numbers of tunnels and voids respectively. $\beta_3(U)$ is zero except for the case of uniform state. The sequence of $\beta_k(U)$ can be estimated using CHomP (computational homology project) software from cubical complexes approximating U [23]. Here, the well-known Euler characteristic χ is obtained as the alternate sum of the sequence of the Betti numbers: $\chi=\beta_0-\beta_1+\beta_2-\beta_3$.

In this paper, we confirm that the combination of RMC modeling method for 2D scattering patterns and the identification method based on recent mathematics is appropriate to study complex 3D morphology and its structural change. In the next section, RMC analysis for tomographical patterns of 2D structure functions and computation of the Betti number are briefly described. In Sec. III, we present the results of RMC analysis for 2D patterns of the structure of particles forming a DG morphology and evaluate the obtained results in terms of the Betti numbers. In the last section, discussion and summary are presented.

II. METHODS

A. Reverse Monte Carlo analysis for two-dimensional tomographical patterns

Reverse Monte Carlo (RMC) analysis is widely used as a general method for analyzing diffraction data of disordered materials [4–6]. The RMC method models a 3D morphology in real space, that is, atomic configurations, from a measured structure factor $S^{\mathrm{exp}}(q)$. In the RMC procedure, the difference between observed structure factor and that calculated from the 3D configuration of virtual atoms in a computer is minimized within the error limit. The concept of the RMC method can be easily extended to analyze the multiple 2D patterns $S(\boldsymbol{q}^{\perp})$ of the structure factors. In order to identify the 3D structure of particles, it is considered that a certain special set of 2D scattering patterns, tomographically observed in crystallographic directions, is required.

To perform RMC analysis, we should consider how we compute 2D scattering pattern of structure factor. Experimentally observed scattering patterns correspond to the 2D patterns $S(\boldsymbol{q}^{\perp})$ when $q^{\parallel}$ is zero or a constant. In a computer, 2D patterns $S(\boldsymbol{q}^{\perp})$ of structure factors are calculated from the positions of virtual atoms. In the RMC method, periodic boundary condition (PBC) are applied. For a certain unit cell, the structure factor is given by

$$S(\boldsymbol{q}) = S_{\mathrm{Inter}}(\boldsymbol{q}) \cdot S_{\mathrm{unitcell}}(\boldsymbol{q}). \tag{1}$$

$S_{\mathrm{Inter}}(\boldsymbol{q})$ is described by delta functions corresponding to Bragg peaks of this particular unit cell. $S_{\mathrm{unitcell}}(\boldsymbol{q})$ is the structure factor of virtual atoms in the unit cell. It can be expressed as

$$S_{\mathrm{Inter}}(\boldsymbol{q}) = \sum_{j_h,j_k,j_l} \exp(i\boldsymbol{q}\cdot\boldsymbol{L}_h j_h)\exp(i\boldsymbol{q}\cdot\boldsymbol{L}_k j_k)\exp(i\boldsymbol{q}\cdot\boldsymbol{L}_l j_l), \tag{2}$$

where $\boldsymbol{L}_h$ denotes the primitive vector of this unit cell in the h direction. Each summation for j_h, j_k, and j_l is a Dirichlet kernel. It is rewritten as

$$\sum_{j_h} \exp(i\boldsymbol{q}\cdot\boldsymbol{L}_h j_h) = \lim_{N_h\to\infty} \frac{\sin[(2N_h+1)\boldsymbol{q}\cdot\boldsymbol{L}_h/2]}{\sin[\boldsymbol{q}\cdot\boldsymbol{L}_h/2]}, \tag{3}$$

where N_h is the number of repeat unit cells in the h direction. The function $S_{\mathrm{Inter}}(\boldsymbol{q})$ is termed as the Laue function. For $N_h\to\infty$, this function becomes the sum of delta functions. For large N_h, the broadening of peaks is negligible. In general RMC methods, including *RMCpow* and *RMCprofile*, a supercell, which consists of many repeated unit cells, is used as a box of PBC. Structure factors are calculated from pair distribution functions of atoms in this supercell. In real experiments of soft materials, the reasons for the broadening of peaks are assumed to be due to the fluctuation of the primitive vectors of the unit cell and width distribution of domain parts of the DG structure in addition to the finite size effect. Since the reconstruction of a certain unit structure belongs to the $Ia\bar{3}d$ space group, we use only the positions of the Bragg peaks, such as the delta functions given by the infinite lattice sum. In this paper, we study an extended RMC method to reconstruct complex network structures such as the DG morphology of real soft materials. In the same manner as in the case of the general RMC methods, the structure factor is calculated from pair distribution functions of large configurations consisting of unit cells repeated many times. The number N_h of repeats can be determined from the condition that peak broadening due to finite size effects is smaller than for that which caused the other effects.

A brief summary of the simulation procedure of RMC for a series of $S_{[hkl]}(\boldsymbol{q}^{\perp}_{[hkl]})$ is as follows: (i) Simulation starts with the initial configuration of particles in a box under PBC in the x, y, and z directions. (ii) A particle and a displacement vector of a trial move are chosen randomly, where the vector satisfies some physical constrains, such as a volume exclusion of particles. (iii) First, a radial distribution function $g_{[hkl]}(\boldsymbol{r}^{\perp}_{[hkl]})$ is calculated from the configuration of particles. Then, the corresponding $S^{\mathrm{calc}}_{[hkl]}(\boldsymbol{q}^{\perp}_{[hkl]})$ are calculated by 2D Fourier transformation (FT) of $g_{[hkl]}(\boldsymbol{r}^{\perp}_{[hkl]})$. The difference $\Delta(\chi^2)$ of the goodness-of-fit parameter χ^2 in each move is calculated, where

$$\chi^2 = \sum_{\langle hkl\rangle} \sum_{\boldsymbol{q}^{\perp}_{[hkl]}\neq\boldsymbol{0}} \Delta[S^2_{[hkl]}(\boldsymbol{q}^{\perp}_{[hkl]})]/\sigma^2_{\mathrm{std}}, \tag{4}$$

$\Delta[S^2_{[hkl]}(\boldsymbol{q}^{\perp}_{[hkl]})]=[S^{\mathrm{exp}}_{[hkl]}(\boldsymbol{q}^{\perp}_{[hkl]})-S^{\mathrm{calc}}_{[hkl]}(\boldsymbol{q}^{\perp}_{[hkl]})]^2$ and σ_{std} is the standard deviation. (iv) For $\Delta(\chi^2)\leq 0$, every trial move is accepted. Trial moves that worsen the fit $[\Delta(\chi^2)>0]$ are accepted with a probability $P=\exp[-\Delta(\chi^2)/2]$. (v) Steps ii–iv are repeated until χ^2 converges. These calculations require huge computing resources. In order to reduce computing

times and memory, the programming code is parallelized with message passing interface (MPI) and is highly optimized for execution on the Earth Simulator, NEC SX-7, SGI Altix 4700 and Hitachi SR11000 machines.

B. Computation of the Betti numbers of morphology formed by particles

In order to characterize the morphology of particles, whose positions are determined by RMC analysis, estimation of the sequence of the Betti numbers is a useful method. Connectivity of the DG morphology is identified by the sequence of the Betti numbers. The Betti numbers of the cubical set U under the PBC can be estimated via linear algebra, where the cubical set U is written using the binary mesh data. Recent advances in algorithms for rapid computation make this a feasible mathematical tool of the CHomP software [23]. In order to use this mathematical tool, we have to connect the particle configurations to the cubical set. In this paper, the cubical set is estimated from the particle configuration as follows. First, the mesh field data of the local number density u_{ijk} is obtained from positions of the center of mass of the particles, where the notation ijk is the index of a lattice point in the rectangular grids. Second, the domain part U^+ of the morphology formed by particles is obtained by the conversion to binary values with binary threshold being b. The resulting image is represented by a cubical set of U^+: $=\{ijk \in [0:N)^3 | u_{ijk} \geq b\}$ consisting of a finite union of cubes. Here, N^3 means number of lattice points under the PBC. The matrix part U^- is also defined by that for $u_{ijk} < b$. Actually, the values of N and b are determined by the heuristic search. The value of N should be smaller than L/σ, because the binary mesh data is generated from the positions of the center of mass of the particles. Here, L is the dimension of a simulation box under PBC and σ is the diameter of particles. In order to study the backbone structure of aggregating particles, it seems to be good that the value of b is equal to the mean volume fraction or a little larger. Details will be described in the next section. The Betti numbers for U^+ and U^- of one-period DG morphology are given as $\beta_k(U^+) = (2,10,0,0)$ and $\beta_k(U^-) = (1,10,1,0)$, respectively. Hereafter, we note the Betti number sets of the DG morphology by $\beta_k(DG^{\pm})$.

III. RESULTS AND DISCUSSIONS

A. Double gyroid morphology and its scattering patterns

As the first test to evaluate the extended RMC analysis for tomographical scattering patterns of complex 3D morphologies, a double gyroid morphology is examined. We studied four sets of light directions $[hkl]$ for tomographical 2D patterns $S_{[hkl]}(\boldsymbol{q}^{\perp}_{[hkl]})$ of structure factors of the DG morphology. The first set is 4 directions of $\langle 111 \rangle$, because scattering patterns in the [111] direction have also been shown frequently in experimental observations [18,19]. The second set is the 18 directions consisting of 6 directions given by $\langle 110 \rangle$ and 12 directions by $\langle 311 \rangle$, because scattering patterns in the [110] and [311] directions have been observed in the experiment by Imai *et al.* [1]. The third is another 18 directions using $\langle 211 \rangle$ instead of $\langle 311 \rangle$; scattering patterns in the [211] direction have been discussed by Vigild *et al.* [20]. As explorations for the smaller number case, the case of 3 directions of $\langle 100 \rangle$ is also examined.

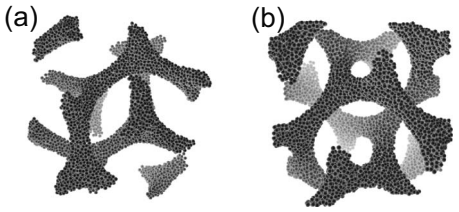

FIG. 1. Snapshots of the reference configuration of a DG morphology as viewed from the [111] and [100] axes, respectively. Two domains form a bicontinuous network that coexists in 3D space.

In order to calculate $S_{[hkl]}(\boldsymbol{q}^{\perp}_{[hkl]})$, we create the model of double gyroid structure consisting of particles. A DG morphology can be closely approximated by the level surface representation. Thus we can get the double gyroid structure by randomly placing the particles in this box satisfying the inequality [24]

$$\begin{aligned} 3 < 2.75[&\sin(4\pi x)\sin(2\pi z)\cos(2\pi y) \\ &+ \sin(4\pi y)\sin(2\pi x)\cos(2\pi z) \\ &+ \sin(4\pi z)\sin(2\pi y)\cos(2\pi x)] - [\cos(4\pi x)\cos(4\pi y) \\ &+ \cos(4\pi y)\cos(4\pi z) + \cos(4\pi z)\cos(4\pi x)], \end{aligned} \tag{5}$$

where (x,y,z) are positions normalized to $[0,1)$ in the box of the PBC. In practice, we set the unit cell of a DG structure composed of 8192 particles, whose diameter σ is equal to 100 nm, in a simulation box of side length $L=4$ μm, under PBC with a volume fraction of 6.7%. Snapshots of the 3D structures obtained by the above method are shown in Fig. 1. Here, the presented figures are sections corresponding to the characteristic directions ([111] and [100]). We can see one well-known recognizable pattern described as wheel patterns in the [111] direction [Fig. 1(a)].

Before the calculation of the pair distribution functions $g_{[hkl]}(\boldsymbol{r}^{\perp}_{[hkl]})$ and the 2D scattering patterns $S_{[hkl]}(\boldsymbol{q}^{\perp}_{[hkl]})$, we estimate the number N_h of repeats of unit cells. We compared structure factors calculated from pair distribution functions of large configurations repeated 2, 4, 8, and 16 times. Here, the grid spacing is set to $\Delta r \simeq 33.3$ nm to calculate $g_{[hkl]}(\boldsymbol{r}^{\perp}_{[hkl]})$ and $\Delta q \simeq 1.67 \times 10^{-4}$ nm^{-1} to transform from $g_{[hkl]}(\boldsymbol{r}^{\perp}_{[hkl]})$ to $S_{[hkl]}(\boldsymbol{q}^{\perp}_{[hkl]})$. For the cases of 8 and 16 periods, peak broadening seems to be similar. In the case of 8 periods, peak broadening by finite size effects seems to be negligibly small. On the other hand, broadening due to finite size effects for the cases of 2 and 4 periods is significant. It is considered that peak broadening is caused by the nonzero width of the domain part of the DG structure for the case of 8 periods. Thereafter, $g_{[hkl]}(\boldsymbol{r}^{\perp}_{[hkl]})$ computed from the large structure with the unit cell of PBC repeated 8 times, PBC is used to transform to $S_{[hkl]}(\boldsymbol{q}^{\perp}_{[hkl]})$. The 2D patterns of structure functions $S_{[hkl]}(\boldsymbol{q}^{\perp}_{[hkl]})$ of the unit cell of the DG morphology, as viewed from $[hkl]$ $=$[110], [111], [211], and [311] axes, are shown in Fig. 2.

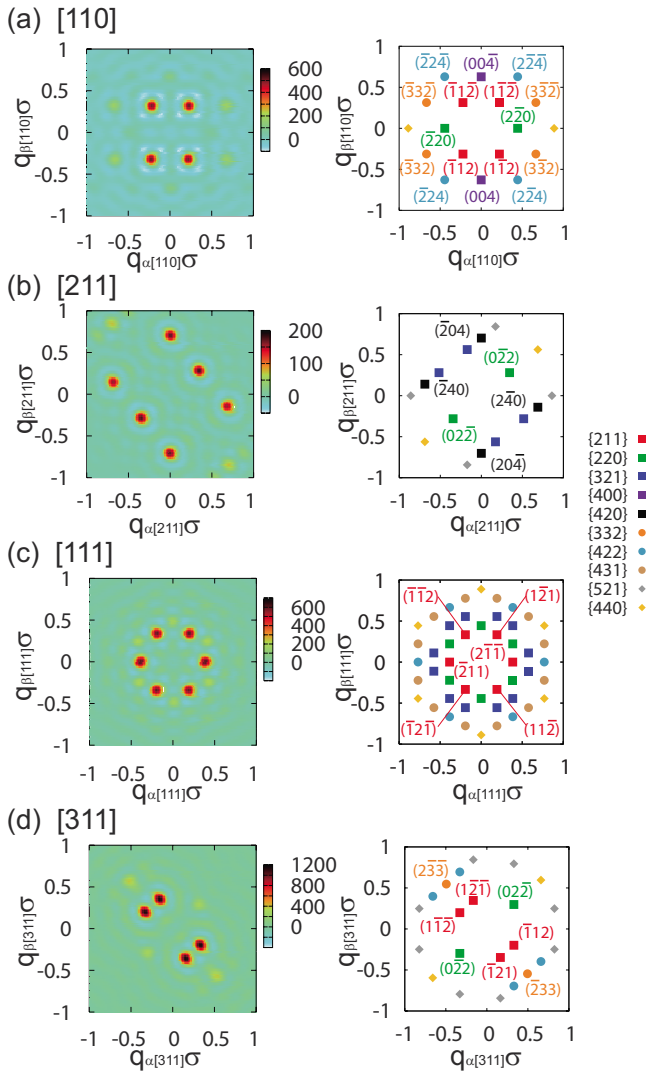

FIG. 2. (Color online) Structure functions $S_{[hkl]}(\boldsymbol{q}^{\perp}_{[hkl]})$ of the DG morphology as viewed from the [110], [211], [111], and [311] axes. The right column shows the corresponding diffraction patterns of peaks of the first ten allowed reflections expected for single crystals of the $Ia\bar{3}d$ phase.

The corresponding diffraction patterns of the peaks of the first 20 allowed reflections expected for single crystals of the $Ia\bar{3}d$ phase are given in Ref. [20]. The first 10 peaks are also depicted in Fig. 2.

B. Reverse Monte Carlo analysis

We focus on the issue of how extended RMC analysis for multiple 2D scattering patterns can reconstruct the complex 3D morphology with topological accuracy. We examine the one-period structure consisting of 8192 particles due to the limitation of our computational resources. An initial configuration is given by a configuration obtained from the molecular dynamics simulation of hard sphere systems. The maximum length $r_{\max}$ of trial moves is set to 100 nm. In the RMC procedure, standard deviation is set to a constant $\sigma_{\mathrm{std}}=10^{-4}$.

The present simulation of the RMC analysis runs up to at least 300 Monte Carlo steps (MCSs), where one MCS means one trial per segment. The elapsed time for one run is a few weeks using four nodes (64CPUs) of a Hitachi SR11000 machine. In this manner, the value of χ^2 converges to a sufficiently small value, which is expected to correspond to an equilibrium state of the system. We recognize that sometimes it does not converge to the DG morphology at 300 MCSs due to a given initial configuration or random numbers or both. As the aim of the present paper is to show possibilities of RMC reconstruction from multiple 2D scattering patterns and an application of the topological identification, we used different sequences of random numbers. When one of the results of a few trial runs seemed to converge to the DG morphology upon visual inspection, we examined it thoroughly. The obtained 2D scattering patterns seem to be similar to the reference $S_{[hkl]}(\boldsymbol{q}^{\perp}_{[hkl]})$ as shown in Figs. 3(a) and 3(b).

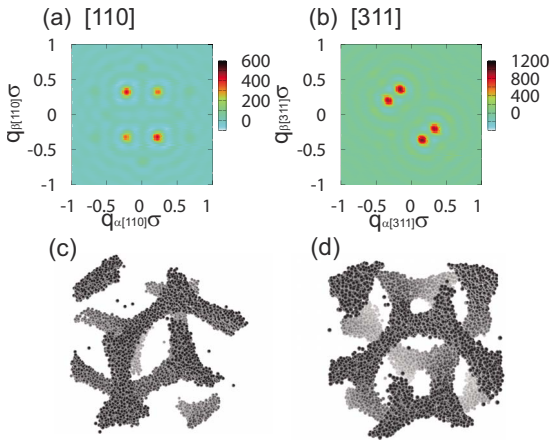

FIG. 3. (Color online) (a) and (b) Structure functions $S_{[hkl]}(\boldsymbol{q}^{\perp}_{[hkl]})$ of the DG morphology viewed from the [110] and [311] axes. (c) and (d) The particle configurations obtained by RMC analysis for tomographical patterns of ⟨110⟩+⟨311⟩. Snapshots as viewed from the [111] and [100] axes are presented.

As shown in the corresponding visualization of Figs. 3(c) and 3(d), it seems that the RMC analysis gives good reconstructions for the case of ⟨110⟩+⟨311⟩ as well as for ⟨111⟩. The RMC reconstructions fail for the cases of ⟨110⟩+⟨211⟩ and ⟨100⟩ as shown in Fig. 4. In general, it is considered that the reasons for the failures are unsuitable conditions or insufficient simulation length.

The method of identification of the DG morphology in this subsection is merely visualization, not morphological analysis. We cannot be sure whether it is possible to distinguish the DG morphology by visual inspection. In the next subsection, we investigate the sequences of the Betti numbers for topological validation of the obtained particle configurations.

C. Topological identification via the Betti numbers

Table I shows the time series of the Betti numbers for the case of ⟨111⟩. It is topologically confirmed that the DG morphology is obtained as the equilibrium configuration of the RMC procedure, because the Betti numbers converge to $\beta_k(DG^{\pm})$ over about 150 MCSs. The sequences of the Betti

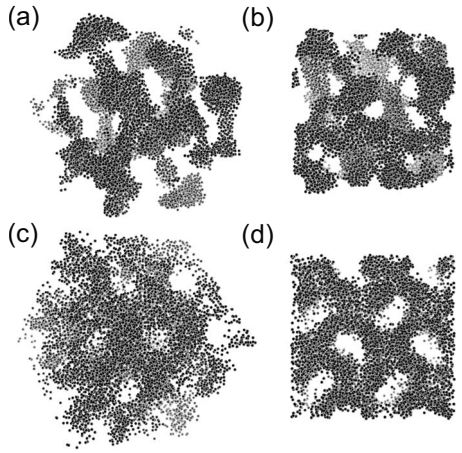

FIG. 4. (a) and (b) Snapshot of the configuration obtained by RMC analysis for tomographical patterns of ⟨110⟩+⟨211⟩. The figures as viewed from the [111] and [100] axes are presented. (c) and (d) Snapshot for ⟨100⟩. The figures as viewed from the [111] and [100] axes are presented.

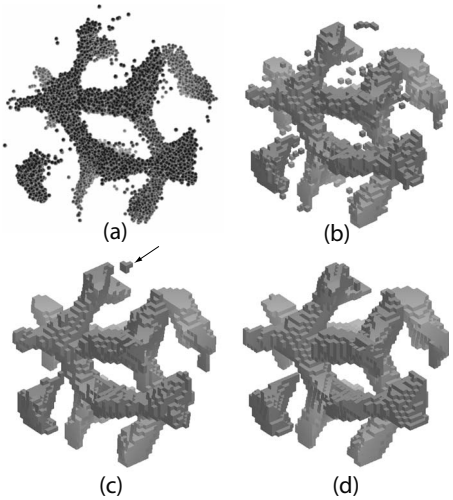

FIG. 5. Typical schematics during the procedure to extract the robust domain structure from the particle configuration obtained by RMC analysis for the case of ⟨111⟩ in case 2b. (a) The obtained particle configuration. (b) Cubical sets converted from the mesh field data with $b=\bar{u}$. (c) The fundamental disordered components are removed by using the Fourier filter and the Betti number sets are obtained as $\beta_k(U_1^+)=(4,10,0,0)$ and $\beta_k(U_1^-)=(1,10,3,0)$. We can guess that there would be a few isolated clusters. Setting $b=2\bar{u}$, the obtained configuration is recognized as the DG morphology. Actually, $\beta_0(U_1^+ \cup U_2^+/U_2^+)=2$ shows that two superfluous isolated rumps are deleted in (d).

numbers are estimated from the mesh field data derived from the obtained particle configurations, where the length of the box of the PBC is divided into $N=2^5$ mesh cubes. Here, the mean volume fraction is set to $\bar{u}\approx 0.067$. However, as shown in Figs. 3(c) and 3(d), the stochastic procedure of the RMC analysis causes the creation of uncontrolled transient local objects such as isolated aggregates. The topological identification is sensitive to isolated clusters and vacancies, and small loops on the roughening interface, i.e., one cube (respectively, one vacancy) adds one to β_0 (respectively, β_2), and one loop adds one to β_1. As one of the aims of this paper is to show how the topological invariants of the robust domain structure can be determined, the transient objects should be removed. For a practical use of the topological identification, verification by some empirical treatments is meaningful although the validity of these empirical treatments is an open question. In order to avoid the checkered cube configurations, we employ the Fourier filter that removes the corresponding high wave number disorder components. Typical situations obtained for Case 2b (to be described in the next subsection) are depicted in Fig. 5. The binary threshold b is set to higher than the mean number density $\bar{u}$ to extract the robust part of the domain structure.

Table II shows the times series of the Betti numbers for the case of ⟨111⟩, in which we employ the twice binary threshold of $b=2\bar{u}$. We found that the numbers of MCSs needed to converge to $\beta_k(DG^{\pm})$ is reduced. It means that the robust part of the domain structure is formed in the early stages of the RMC procedure.

The time series of the Betti numbers for the case of ⟨110⟩+⟨311⟩ are also shown in Table III, where the convergence numbers are $\beta_k(U_1^{\pm})=(1,12,0,0)\neq\beta_k(DG^{\pm})$. As shown in the corresponding visualization of Fig. 6(a), however, it may be recognized as the DG morphology. We can guess intuitively that two gyroid network domains would be connected by a superfluous connection. Hereafter, $U_{1,2}^{\pm}$ denotes the domain and matrix part of the cubic set obtained with $b=\bar{u}$ and $2\bar{u}$, respectively. Consequently, by doubling the threshold, we obtained $\beta_k(U_2^{\pm})=\beta_k(DG^{\pm})$ as shown in Table IV and Fig. 6(b). The first relative Betti number, i.e., rank of the first relative homology groups, is computed as $\beta_1(U_1^+ \cup U_2^+/U_2^+)=3$ using CHomP software [23]. It confirms that three superfluous connections will be deleted, i.e., one of

TABLE I. Time series of the Betti numbers sequence for the case of ⟨111⟩ with $b=\bar{u}$.

MCSs	$\beta_0(U_1^+)$	$\beta_1(U_1^+)$	$\beta_2(U_1^+)$	$\beta_0(U_1^-)$	$\beta_1(U_1^-)$	$\beta_2(U_1^-)$
30	1	21	0	1	20	0
60	1	16	0	1	13	0
90	1	14	0	1	12	0
120	1	10	0	1	10	1
150	2	10	0	1	10	1
180	2	10	0	1	10	1

TABLE II. Time series of the Betti numbers sequence for the case of ⟨111⟩ with $b=2\bar{u}$.

MCSs	$\beta_0(U_2^+)$	$\beta_1(U_2^+)$	$\beta_2(U_2^+)$	$\beta_0(U_2^-)$	$\beta_1(U_2^-)$	$\beta_2(U_2^-)$
10	15	0	0	1	3	15
20	2	5	0	1	6	2
30	1	14	0	1	10	1
40	1	10	0	1	10	1
50	1	10	0	1	10	1
60	2	10	0	1	10	1

TABLE III. Time series of the Betti numbers sequence for the case of $\langle 110\rangle+\langle 311\rangle$ with $b=\bar{u}$.

MCSs	$\beta_0(U_1^+)$	$\beta_1(U_1^+)$	$\beta_2(U_1^+)$	$\beta_0(U_1^-)$	$\beta_1(U_1^-)$	$\beta_2(U_1^-)$
50	1	20	0	1	19	0
100	1	19	0	1	16	0
150	1	14	0	1	13	0
200	1	12	0	1	12	0
250	1	12	0	1	12	0
300	1	12	0	1	12	0

TABLE IV. Time series of the Betti numbers sequence for the case of $\langle 110\rangle+\langle 311\rangle$ with $b=2\bar{u}$.

MCSs	$\beta_0(U_2^+)$	$\beta_1(U_2^+)$	$\beta_2(U_2^+)$	$\beta_0(U_2^-)$	$\beta_1(U_2^-)$	$\beta_2(U_2^-)$
50	1	11	0	1	11	0
100	1	11	0	1	11	0
150	1	10	0	1	10	2
200	2	10	0	1	10	1
250	2	10	0	1	10	1
300	2	10	0	1	10	1

them connects two network gyroid domains into one and the other two connections cause two loop defects. The relative homology $H_k(A\cup B/B)$ is equal to the regular homology of the quotient space $A\cup B/B$, i.e., the topology of $A\cup B$ modulo B. The mathematical tools which we use here are by no means novel. A more complete treatment can be found in Ref. [22]. In our case, $\beta_1(A\cup B/B)=1$ (respectively, $\beta_0(A\cup B/B)=1$) provides us with the information about a superfluous connection (respectively, an isolated cluster).

We also examine how the RMC reconstructions go wrong for the cases of $\langle 110\rangle+\langle 211\rangle$ and $\langle 100\rangle$. The associated time series of the Betti number sequences are presented in Tables V and VI. The time change behavior for the case of $\langle 110\rangle+\langle 211\rangle$ differs from that for $\langle 100\rangle$. The Betti numbers quickly converge into stationary values shown in Table VI along with the convergence of χ^2, while the Betti numbers in Table V seem to be in a halfway state through the DG morphology. It is considered that the behavior of the Betti numbers shown in Table VI would indicate that three 2D scattering patterns are not sufficient as conditions for RMC reconstructions. On the other hand, we suspect that the reason for the unsuccessful reconstruction in the case of $\langle 110\rangle+\langle 211\rangle$ is insufficient Monte Carlo steps. Thus the scattering patterns of the [211] direction are not suitable for quantitative determination of the structure from experimental data. Comparing the 2D scattering patterns shown in Fig. 2, the intensities of the highest peaks in the [211] direction are weaker than those in [110], [111], and [311], because peaks corresponding to {211} are not observed in the [211] direction. Here, the amplitude of peaks corresponding to {211} is about ten times stronger than that to {220}. It is obvious that, in order to perform topological identification for known structures, 2D scattering patterns in crystallographic directions should be examined in experiments. On the other hand, in order to study unknown structures, e.g., kinetic pathways during the morphological transition, we should deduce proper robust domain structures from low intensity 2D scattering patterns in arbitrary directions. In the next subsection, we will try to improve the RMC fitting process to reconstruct the DG morphology from 2D scattering patterns including with relatively low intensity patterns in the $\langle 211\rangle$ directions.

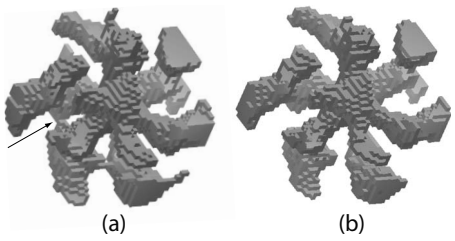

FIG. 6. Typical schematics of the extraction of the robust part of the domain structure for the case of $\langle 110\rangle+\langle 311\rangle$. (a) Cubical sets converted from the mesh field data with $b=\bar{u}$. To eliminate the thin connection marked with the arrow, the binary threshold is set to be twice as high as in (b).

D. Empirical improvements for fast fitting

In the rest of the paper, in order to realize the reconstruction from weak intensity 2D patterns in the direction $\langle 110\rangle+\langle 211\rangle$, improvements of the fitting process are studied. The control of maximum length $r_{\max}$ of trial moves, size σ_{ev} of excluded volume constraints, and / or value σ_{std} of standard deviations are important to do this. In this subsection, we examine the effect by the controlling $r_{\max}$ and σ_{ev} as a preliminary study. According to the conventional treatments of RMC analysis, it is expected that the small $r_{\max}$ value would reduce the transient local objects generation. The control of σ_{std} is not considered because the scattering data used are calculated from the computer-generated configuration and the σ_{std} value in real experiments should be determined from experimental conditions. As the first example, we examine three cases with a controlled $r_{\max}$ for $\sigma_{\mathrm{ev}}=100$ nm as follows:

Case 1a. 800 nm up to 50 MCSs, 400 nm up to 100 MCSs, 200 nm up to 150 MCSs, and 100 nm over 150 MCSs.

Case 1b. 400 nm up to 50 MCSs, 200 nm up to 100 MCSs, and 100 nm over 100 MCSs.

TABLE V. Time series of the Betti numbers sequence for the case of $\langle 110\rangle+\langle 211\rangle$.

MCSs	$\beta_0(U_2^+)$	$\beta_1(U_2^+)$	$\beta_2(U_2^+)$	$\beta_0(U_2^-)$	$\beta_1(U_2^-)$	$\beta_2(U_2^-)$
50	5	5	0	1	3	8
100	3	10	0	1	5	5
150	3	6	0	1	8	4
200	2	2	0	1	3	4
250	1	4	0	1	4	3
300	1	3	0	1	7	3

TABLE VI. Time series of the Betti numbers sequence for the case of ⟨100⟩.

MCSs	$\beta_0(U_2^+)$	$\beta_1(U_2^+)$	$\beta_2(U_2^+)$	$\beta_0(U_2^-)$	$\beta_1(U_2^-)$	$\beta_2(U_2^-)$
50	13	0	0	1	3	20
100	17	0	0	1	3	21
150	17	0	0	1	3	22
200	17	0	0	1	3	22
250	17	0	0	1	3	22
300	17	0	0	1	3	22

Case 1c. 200 nm up to 50 MCSs and 100 nm over 50 MCSs.

In order to examine the robust part of the domain structure, we set the binary threshold to $b=2\bar{u}$. Numbers of MCSs to converge to the DG morphology are shown in Table VII. For the cases of ⟨111⟩ and ⟨110⟩+⟨311⟩, the MCS number has a tendency to be smaller than that for constant $r_{\max}=100$ nm. Although we recognize the dispersion of the values of MCSs which converge to the reference morphology, we note that large values of $r_{\max}$ seem to be meaningful. In order to confirm this claim, we should examine many cases with different σ_{ev} and directions, although it is difficult to compute them at the present time due to a huge requirement of computational resources.

In order to consider effects arising from the size of the excluded volume constraints, we also examine the following three cases controlling $r_{\max}$ for $\sigma_{\mathrm{ev}}=50$ nm as follows:

Case 2a. the maximum length $r_{\max}$ is fixed to 50 nm.

Case 2b. 200 nm up to 50 MCSs, 100 nm up to 100 MCSs, and 50 nm over 100 MCSs.

Case 2c. 400 nm up to 50 MCSs, 200 nm up to 100 MCSs, 100 nm up to 150 MCSs, and 50 nm over 150 MCSs.

Numbers of MCSs needed to converge into the DG morphology are shown in Table VIII. For the case of ⟨110⟩+⟨211⟩, the RMC reconstruction goes well except for $r_{\max}=50$ nm. It is remarkable that RMC analysis for the case of ⟨110⟩+⟨211⟩ is successful even though the intensity of the 2D patterns for ⟨211⟩ is considerably weaker than that for ⟨311⟩. We can conclude that decreasing the size of σ_{ev} seems to be effective when used with large $r_{\max}$. We expect that this scheme is powerful analyzing real experimental data, especially the kinetic pathway during the morphological transition via the DG morphology [1,20], because our results indicate the possibility of 2D tomographical pattern RMC analysis for lights in the arbitrary directions.

TABLE VII. Numbers of Monte Carlo steps (MCSs) needed to converge to the DG morphology when σ_{ev} is set to 100 nm. The symbol "—" indicates the cases where the Betti numbers of all configurations of a few trials with different sequences of random numbers do not converge to $\beta_k(DG^{\pm})$ until 300 MCSs.

	Maximum move	⟨111⟩	⟨110⟩ ⟨311⟩	⟨110⟩ ⟨211⟩
Case 1a	800 nm	20 MCSs	50 MCSs	—
Case 1b	400 nm	40 MCSs	40 MCSs	—
Case 1c	200 nm	180 MCSs	20 MCSs	—

TABLE VIII. Numbers of MCSs needed to converge to the DG morphology when σ_{ev} is set to 50 nm. The symbol "—" indicates the case where the configuration does not converge to $\beta_k(DG^{\pm})$ within 300 MCSs.

	Maximum move	⟨111⟩	⟨110⟩ ⟨311⟩	⟨110⟩ ⟨211⟩
Case 2a	50 nm	100 MCSs	30 MCSs	—
Case 2b	200 nm	70 MCSs	30 MCSs	50 MCSs
Case 2c	400 nm	30 MCSs	20 MCSs	30 MCSs

IV. SUMMARY

In this paper, we present the validity of a different modeling method by 2D pattern reverse Monte Carlo analysis for tomographically observed two-dimensional patterns $S_{[hkl]}(\boldsymbol{q}^{\perp}_{[hkl]})$. It is confirmed that 2D pattern RMC analysis can reconstruct a DG morphology from $S_{[hkl]}(\boldsymbol{q}^{\perp}_{[hkl]})$ for appropriate multiple directions. From our numerical experiments, we can conclude the following. When only 2D scattering patterns consist mainly of strong peaks associated with {211} are used as the reference scattering patterns RMC reconstructions go well. When weak 2D scattering patterns such as those in the directions of ⟨211⟩ are included in the set of the reference scattering patterns, long RMC steps are required to converge to the reference structure. Control of maximum length $r_{\max}$ of trial moves and size σ_{ev} of the excluded volume interaction is effective for fast RMC reconstructions. In order to evaluate the topological feature of the robust parts of the domain structure, empirical treatments such as adjusting binary threshold and applying Fourier filter are useful. Computational homology also provides us with definitive identification of topological classification among the complex morphologies obtained from experimental observation and numerical simulations. In future studies, we should examine the essential factors involved in RMC reconstruction conditions and the validity of the empirical treatments with which to generate cubical sets before computing the Betti numbers by using mathematical techniques.

In the preliminary study for the double diamond (DD) morphology, which belongs to the $Pn\bar{3}m$ space group, we succeed in the RMC reconstruction with 2D scattering patterns for the six directions of ⟨110⟩. Here, the Betti numbers of one-period DD morphology are given as $\beta_k(U^+)=(2,18,0,0)$ and $\beta_k(U^-)=(1,18,1,0)$. With the 2D pattern RMC method and computational homology, it is now possible to reconstruct complicated 3D morphology from scattering patterns and to quantitatively measure the connectivity of complex network domains. These results suggest that the combination of RMC and CHomP will provide a new and useful approach for connecting scattering experiments to theoretical 3D morphology images.

ACKNOWLEDGMENTS

The authors thank Professor T. Arai, H. Kishimoto, Y. Shinohara, Professor M. Imai, and Professor Y. Amemiya for useful discussion about scattering experiments and RMC analysis, Professor Y. Nishiura and Professor W. Kalies for useful discussion about computational homology, and Dr. H. Suno, Dr. H. Hasegawa, Dr. H. Uehara, and S. Shingu for optimization of the programming code. Partial support by a Grant-in-Aid for Exploratory Research 19654015 and Young Scientists (B) 18740238 is acknowledged as well as computational resources from Information Initiative Center (Hokkaido University), Earth Simulator (Japan Agency for Marine-earth Science and Technology), Okazaki National Research Facilities (National Institute of Natural Sciences), and Institute for Solid State Physics (University of Tokyo).

[1] M. Imai, K. Sakai, M. Kikuchi, K. Nakaya, A. Saeki, and T. Teramoto, J. Chem. Phys. **122**, 214906 (2005).
[2] H. Jinnai, Y. Nishikawa, T. Ikehara, and T. Nishi, Adv. Polym. Sci. **170**, 115 (2004).
[3] Y. Shinohara, H. Kishimoto, K. Inoue, Y. Suzuki, A. Takeuchi, K. Usugi, N. Yagi, K. Muraoka, T. Mizoguchi, and Y. Amemiya, J. Appl. Crystallogr. **40**, S397 (2007).
[4] R. L. McGreevy and L. Pusztai, Mol. Simul. **1**, 359 (1988).
[5] D. A. Keen and R. L. McGreevy, Nature (London) **344**, 423 (1990).
[6] R. L. McGreevy, J. Phys.: Condens. Matter **13**, R877 (2001).
[7] K. Hagita, T. Arai, M. Inui, K. Matsuda, and K. Tamura, J. Appl. Crystallogr. **40**, S544 (2007).
[8] L. Pusztai, H. Dominguez, and O.A. Pizio, J. Colloid Interface Sci. **277**, 327 (2004).
[9] G. Toth, J. Mol. Liq. **129**, 108 (2006).
[10] D. I. Svergun, Biophys. J. **76**, 2879 (1999).
[11] K. Hagita, H. Okamoto, T. Arai, H. Kishimoto, N. Umesaki, Y. Shinohara, Y. Amemiya, in Flow Dynamics: The Second International Conference on Flow Dynamics, AIP Conf. Proc. No. 832, edited by M. Tokuyama and S. Maruyama (AIP, Melville, NY, 2006), p. 368.
[12] K. Hagita, T. Arai, H. Kishimoto, N. Umesaki, Y. Shinohara, and Y. Amemiya, J. Phys.: Condens. Matter **19**, 335217 (2007).
[13] H. M. Rietveld, J. Appl. Crystallogr. **2**, 65 (1969).
[14] M. Sakata and M. Sato, Acta Crystallogr., Sect. A **46**, 263 (1990).
[15] A. Mellergard and R. L. McGreevy, Acta Crystallogr., Sect. A **55**, 783 (1999).
[16] D. A. Keen, M. G. Tucker, and M. T. Dove, J. Phys.: Condens. Matter **17**, S15 (2005).
[17] E. L. Thomas, D. M. Anderson, C. S. Henkee, and D. Hoffman, Nature (London) **334**, 598 (1988).
[18] D. A. Hajduk, P. E. Harper, S. M. Gruner, C. C. Honeker, G. Kim, E. L. Thomas, and L. J. Fetters, Macromolecules **27**, 4063 (1994).
[19] M. F. Schulz, F. S. Bates, K. Almdal, and K. Mortensen, Phys. Rev. Lett. **73**, 86 (1994).
[20] M. E. Vigild, K. Almdal, K. Mortensen, I. W. Hamley, J. P. A. Fairclough, and A. J. Ryan, Macromolecules **31**, 5702 (1998).
[21] T. Teramoto and Y. Nishiura, J. Phys. Soc. Jpn. **71**, 1611 (2002).
[22] T. Kaczynski, K. Mischaikow, and M. Mrozek, *Computational Homology*, Applied Mathematical Science No. 157 (Springer-Verlag, New York, 2004).
[23] W. Kalies and P. Pilarczyk, Computational Homology Project, http://chomp.rutgers.edu
[24] D. Hoffman, J. Hoffman, and M. Weber, The Scientific Graphics Project, http://www.msri.org/about/sgp/SGP